Intermediate Conversion Kinetics in Ticalcium Aluminate Formation

Chinmay Ghoroi
Indian Institute of Technology Bombay, Dept. of Chemical Engineering, Powai, Mumbai 400 076, India

A. K. Suresh
Indian Institute of Technology Bombay, Dept. of Chemical Engineering, Powai, Mumbai 400 076, India

DOI 10.1002/aic.11220
Published online July 25, 2007 in Wiley InterScience (www.interscience.wiley.com).

Solid-solid reactions are important in many chemical and metallurgical process industries, as also in the semiconductor and electrochemical materials industries. In comparison to their fluid counterparts, these systems are difficult to model with any degree of rigour, but models derived from the fluid-solid literature have often been used with success to interpret the data. There are lacunae, however, and our previous work[1] has shown the inadequacy of the conventional models when reactions take place through a network of some complexity. In that work, the conversion of alumina and calcia to C_3A was shown to be a series network, with $C_{12}A_7$ being the (stable) reaction intermediate. The second reaction step of that network is studied here, namely the conversion of $C_{12}A_7$ to C_3A by reaction with calcia. It has been shown that this reaction takes place in a single step. While conventional wisdom treats such reactions as taking place invariably at a (moving) reaction front, it has been shown that a proper interpretation of data requires cognizance of a volume reaction component, which may, under conditions of severe diffusion limitations, be approximated well by a front reaction.
 AIChE J, 53: 2399–2410, 2007
Keywords: solid-solid reactions, kinetics, shrinking core, volume reaction, contact point model, intermediate

Introduction

Tricalcium aluminate ($Ca_3Al_2O_6$ or C_3A as normally represented in cement chemistry) is one of the important constituents of ordinary Portland cement. In the rotary cement kiln, it forms early and, by melting around 1,350°C and providing a liquid phase, assists in the formation of the other cement phases.[2] During hydration of cement, it acts as a retarder in the reaction between water and calcium silicate phases, and, thus, provides for the required workability. Apart from its use as a cement phase, other applications of C_3A, for example, as a catalyst support,[3] and as a doping material to improve the biocompatibility and bioactivity of calcium aluminate bone cement,[4] have emerged in recent years.

Despite a long history of application, the kinetics of formation of C_3A have eluded consensus and studies continue. The formation of C_3A from the oxides of calcium and aluminium is typical of a series-parallel mechanism exhibited by several solid-phase reactions.[1,5] Various intermediate phases, such as $C_{12}A_7$ ($Ca_{12}Al_{14}O_{33}$) and CA ($CaAl_2O_4$), have been reported in the literature.[6] In our recent studies on the system,[1] the influence on the observed kinetics, of initial conditions and the manner of forming the reactive entity has been highlighted, and it has been shown that $C_{12}A_7$ is the sole intermediate under conditions of good interparticle contact. This intermediate was seen to form in a fast step, and

Correspondence concerning this article should be addressed to A. K. Suresh at aksuresh@che.iitb.ac.in.

convert to the final product C_3A in a relatively slower step. It would greatly aid the understanding of the overall mechanism if each of these steps were understood separately. In particular, the slower second step would be expected to have a greater bearing on the kinetics of the overall reaction. While there are a few studies[7,8] on the formation kinetics of $C_{12}A_7$, no information is available on the conversion kinetics of $C_{12}A_7$ to C_3A. Thus, the main objective of this article is to study the kinetics and mechanism of intermediate conversion in C_3A synthesis, namely, the conversion of $C_{12}A_7$ to C_3A by calcium oxide.

In the field of solid-state reactions, interpretation of kinetic data is usually carried out using simplistic models, often inspired by the fluid-solid literature. One of the reactants is assumed to diffuse into the other reactant, and the reactions are normally assumed to take place at a front that moves inward with time toward the center of the nondiffusing reactant particle. It is a second objective of this work to treat the $C_{12}A_7$ to C_3A conversion as a model reaction to test the applicability of several of the models proposed in the literature. In particular, the question of whether models which consider the reaction to take place *throughout a region* rather than at a front have a place in gas-solid kinetics is examined in some detail. These studies are part of a wider study aimed at establishing theoretical frameworks and experimental protocols for studying multistep solid phase reactions.

Literature

In general, high-temperature solid-phase reactions are controlled by diffusion of one of the components into the other. For example, in the case of calcia-alumina system, it is generally agreed that CaO is the diffusing species[9,10] — CaO is believed to diffuse through the layers of different calcium aluminate phases to the Al_2O_3 core.[11] The status of kinetic studies on single stage solid-solid reactions upto the late seventies was reviewed by Tamhankar and Doraiswamy.[12] Their review highlighted a clear need for modeling efforts in describing solid-solid reaction kinetics. Apart from the difficulties with the theories, kinetic studies on solid-phase systems are rendered the more difficult, in comparison with their fluid-phase counterparts, by the number of factors which have to be tightly controlled in order to ensure an absence of experimental artifacts and achieve good reproducibility.[1] Such factors include particle size and its distribution,[13–19] the method used to mix the reactants,[1] the degree of homogeneity of the mix, history of any pretreatment, and goodness of interparticle contact. Volume change during reaction[20–24] often adds a further complication to interpretation of data. Many researchers have preferred to study solid-solid reaction kinetics in pellet-pellet systems[25–29] to avoid some of the aforementioned complexities. Reactions in mixed powders is, however, closer to practical usage. Studies addressing some of the aspects in such situations, such as the role of the particle geometry and surface contacts,[30] the influence of molar ratio of the reactant mixture, degree of compactness and ratio of average particle size,[31] are available.

Theoretical models used in the interpretation of experimental kinetics tended to follow developments in the gas-solid reactions in the earlier years. Reactions are often diffusion controlled, and models based on a moving reaction front have been commonly used. The models of Jander,[32] Ginstling-Brounshtein[33] and Valensi-Carter,[23–24] deserve mention in this *genre*. The moving reaction front models (or "shrinking core" models in the context of a spherical geometry) lead to an equation of the form

$$g(\alpha) = kt \tag{1}$$

where the form of the function $g(\alpha)$ (α being the overall conversion) depends on the model, and k and t are the (relevant) rate parameter and time, respectively. Table 1 lists the more commonly used models of this type (with the corresponding interpretation of the parameter k), with reference to the reaction

$$I(s) + \nu_B B(s) \rightarrow \nu_P P(s) \tag{2}$$

(where I is the immobile reactant, and B, the diffusing species). Note that the function $g(\alpha)$ for the Valensi-Carter model has an additional parameter Z (the ratio of the volume of the product formed per unit volume of the reactant), which accounts for changes in particle size with reaction. More exhaustive lists are available elsewhere.[1,34] Comparative studies on these models for specific systems are available. For example, Beretka,[34] in studies covering a range of particle sizes and reactant ratios on seven different reaction systems, ranks different models of the type of Eq. 1, on the basis of the correlation coefficients of $g(\alpha)$ vs. t plots. Similarly, Mukherjee and Wang,[36] and Watanabe[37] have worked on Bi_2O_3-Fe_2O_3 and BaO_2-Fe_2O_3 systems, respectively, and concluded that Jander's model[32] is the appropriate model for these reaction systems. The applicability of the models can be tested by the reduced plot method of Sharp et al.[38] prior to estimation of the kinetic parameters by fitting the model to the data.[1] In general, diffusion-controlled mechanisms are suggested by such comparisons, but usually, the models do not fit over the entire conversion range of 0–100%.

The pseudo steady-state assumption, commonly made in treating the diffusion-controlled case in the shrinking-core framework, is easy to justify when the density of the diffusing reactant is much less than that of the other reactant, as is the case with gas-solid reactions. However, the densities are comparable in liquid-solid and solid-solid systems. Ishida et al.[39] have tested the applicability of the pseudo steady-state assumption for moving-boundary problems in spherical particles. They found that the approximation is sufficiently correct with respect to gas diffusion, but may introduce errors when the process is controlled by heat transfer. Lindman and Simonsson[40] have tested the validity of pseudo

Table 1. Common Models of the Moving Reaction Front Type used in the Interpretation of Solid-Solid Reaction Kinetics

Model	Symbol	$g(\alpha)$	k
Jander	D_3	$\left[1-(1-\alpha)^{\frac{1}{3}}\right]^2$	$2\left(\frac{D_e C_{B0}}{\nu_B R_{I0}^2 C_{I0}}\right)$
Ginstling-Brounshtein	D_4	$\left[1-\frac{2}{3}\alpha-(1-\alpha)^{\frac{2}{3}}\right]$	$2\left(\frac{D_e C_{B0}}{\nu_B R_{I0}^2 C_{I0}}\right)$
Valensi-Carter	VC	$\left[\frac{Z}{Z-1}\right]-(1-\alpha)^{\frac{2}{3}}-\left[\frac{[1+(Z-1)\alpha]^{\frac{2}{3}}}{(Z-1)}\right]$	$2\left(\frac{D_e C_{B0}}{\nu_B R_{I0}^2 C_{I0}}\right)$
Shrinking core with reaction control	R_3	$\left[1-(1-\alpha)^{\frac{1}{3}}\right]$	$2\left(\frac{k_s C_{B0}}{\nu_B R_{I0} C_{I0}}\right)$

steady-state approximation in treating shrinking core model in case of liquid-solid reaction system, and quantified the relative error in calculating the time for a certain conversion as a function of the stoichiometric ratio (q) of liquid reactant concentration to that of solid. For $q = 1$, the relative error in calculating the time is within 5% in the range of 50 – 99% conversion. Often, for liquid-solid systems $q \leq 0.2$, and the relative error is less than 2% over the entire range of conversion. Huang et al.[41] have compared the transient solutions to the shrinking core model with the Ginstling-Brounshtein model.[33] The solutions agree at small times and for diffusion-controlled reaction systems, which quickly reach a steady state. Frade and Cable[42–44] have developed numerical solutions for such moving-boundary situations for solid particles of different shapes. Comparison with Jander (D_3) and Ginstling-Brounshtein (D_4) models showed once again that the assumptions made in the latter models are valid upto a certain conversion (about 60%). The errors are negligible when the immobile reactant has a small solubility in the product layer. They also model the mixed-control case with diffusion and a first-order reaction for spherical, cylindrical and planar particulates.[43] While none these transient models has been tested against data, considering experimental errors, there does not seem to be a case, by and large, for invoking the complexities of unsteady state diffusion in data interpretation.

Unlike the models listed in the table (Table 1) which consider the reaction to take place only at a sharp interface (front-reaction models), there is a case for considering volume reactions in the solid-solid context as well, something that one does not see done in the literature on the subject. Ishida and Wen[45,46] have developed volume reaction models for gas-solid reactions. Here also, two zones will develop beyond a time t_1 which is needed for the solid reactant to be completely converted at the particle surface. For larger times, a boundary will separate the zone of diffusion-reaction (the core) from the zone of pure product (the shell). We may, therefore, divide the reaction time into a "First stage" (before t_1) and a "Second stage" (from t_1 to complete reaction). Ishida and Wen[45] provided the following equations for conversion-time behavior, when the external mass-transfer resistance is negligible

$$\text{First stage}: \quad \alpha = \frac{3}{\phi^2}[\phi\coth(\phi) - 1]k_p C_{B0} t \tag{3}$$

$$\text{Second stage}: \quad \alpha = 1 - \xi_m^3 + \frac{3\xi_m}{\phi^2}[(\phi\xi_m)\coth(\phi\xi_m) - 1] \tag{4}$$

where $\phi = \left(R_{I0}\sqrt{\frac{\nu_B k_P C_{I0}}{D_e}}\right)$ is akin to a Thiele modulus. ξ_m is the dimensionless radius of the boundary between the two regions mentioned previously, and moves inward with time as given by

$$k_P C_{B0} t = 1 + \frac{\phi^2}{6}(1-\xi_m)^2(1+2\xi_m) + (1-\xi_m)[(\phi\xi_m)\coth(\phi\xi_m) - 1] \tag{5}$$

The time for completion of the first stage is given by

$$t_1 = \left(\frac{1}{k_P C_{B0}}\right) \tag{6}$$

For large values of ϕ, the authors show the model to reduce to the Ginstling-Brounshtein model, and in this sense, the volume-reaction model may be considered to be more general than the front-reaction models. As remarked before, the applicability of volume-reaction models to solid-solid reactions does not appear to have been tested.

There have also been attempts in the literature to consider the particulate nature of *both* reactants in solid-solid reactions. The most important of these considers the case of a finite number of points of contact between the reacting particles. Based on the calculations of Ouchiyama and Tanaka[47] for the average number of contact points between randomly mixed solid particles, Hao and Tanaka[48–49] have developed a pseudo steady-state kinetic model for a diffusion controlled reaction, which originates at the contact points, with the reaction fronts gradually moving into the reactant particles. An initial stage of reaction up to the time (t_1), at which two neighboring product zones touch one another can be recognized, and this is termed as the transition period. Both the initial transition period and the post-transition period have been modeled, for unidirectional diffusion[49] and counter diffusion[50] situations. The unidirectional case is more relevant in this context. In this case, conversion of the nondiffusing component (I), during the transition period, is given[49] as

$$\alpha = \left(\frac{\tau}{2} - \frac{3}{16}\tau^{\frac{3}{4}}\right)N_{cp} \tag{7}$$

where τ is the dimensionless time

$$\tau = \left(\frac{3D_e x_1 C_B}{\nu_B R_{I0}^2 C_I}\right)t = Kt \tag{8}$$

and N_{cp} is the average number of contact points between randomly mixed solid particles, given by Ouchiyama and Tanaka,[47] which depends on initial particle radius ratio (ξ_0) and initial volume fraction of the nondiffusing reactant in the randomly packed mixture (X_{VI}). Subsequent to the transition period, the conversion-time relationship is given as

$$\alpha = 1 - \exp(-\kappa\tau^n) \tag{9}$$

where κ and n are the function of number of contact points N_{cp}. Hao and Tanaka[49] and Shimizu and Hao[50] provide equations and charts for finding κ and n.

The contact-point models have been applied for different binary mixtures.[50–52] The authors show that this model gives the same value of the rate parameter across several data sets with different initial molar ratios of the reactants, while the Ginstling-Brounshtein model gives different values. The mathematical treatment makes several approximations on the geometrical details of the reacting particle, the validity of which would be questionable when the number of contact points is small (like two or three). Also, somewhat counterintuitively, it appears that the model does not give the same results as the shrinking core (say Ginstling-Brounshtein) models when the number of contact points becomes very large. None of the reactions important in cement manufacture has been studied using the contact point models.

From the point of view of the mechanisms of conversion, certain interesting structural features of the starting materials

Table 2. Physical Parameters used in the Calculations

[Ref]Parameters	Value	Units
[62]Molar density of CaO (C_{B0})	59.28	kmol m^{-3}
[62]Molar density of $C_{12}A_7$ (C_{I0})	1.94	kmol m^{-3}
[62]Molar density of $CaCO_3$ (C'_{B0})	28.0	kmol m^{-3}
Average radius of $CaCO_3$ (R'_{B0})	1.26×10^{-6}	m
Average radius of $C_{12}A_7$ (R_{I0})	0.88×10^{-6}	m
Initial radius ratio, ξ_0 ($=R'_{B0}/R_{I0}$)	1.42	—
Volume fraction of $C_{12}A_7$ (X_{VI})	0.615	—
[50]Average dimensionless thickness of contact point, x_1	0.05	—
Stoichiometric coefficient (ν_B)	9	—
[63]Z for VC model	1.22	—

may be relevant in this case. $C_{12}A_7$, under normal conditions of its preparation in air in the temperature range of 950°C – 1,350°C, is not a strictly anhydrous compound.[53] The unit cell of $C_{12}A_7$ (space group: $I\bar{4}3d$, with a lattice constant: 1.199nm[54]) consists of two formula units of $C_{12}A_7$ ($[Ca_{24}Al_{28}O_{64}]^{4+}$, $2O^{2-}$) with twelve subnanometer size (~0.4nm) cages.[55–56] Within the crystal structure, there exists an extra-framework of encapsulated O^{2-} ions in the form of O^- or O_2^- or O_2^{2-}, depending on the preparation condition of $C_{12}A_7$. Sushko et al.[56] and Imlach et al.[57] have found that these O^{2-} ions (~0.07 – 1.0%) remain intact even at temperatures of 1,200°C to 1,449°C (the melting point[58] of $C_{12}A_7$). The O^{2-} ions, which are on the surface of the $C_{12}A_7$ structure, readily react with the moisture present in the furnace environment,[59] and $C_{12}A_7$ converts to $Ca_{12}Al_{14}O_{32}(OH)_2$ with a maximum ~1.4% of water content at 950°C.[53,60]

In this study, we have synthesized $C_{12}A_7$ under controlled conditions, and used it, along with CaO prepared from commercial $CaCO_3$, to study the formation kinetics of C_3A. The data have been interpreted using a variety of models, such as the shrinking core model, volume reaction model and contact point model to get some insights into the applicability of the underlying concepts in such cases.

Experimental

$C_{12}A_7$ was synthesized in the laboratory from AR grade $CaCO_3$ and $Al(OH)_3$ gel powder (in 12:14 mole ratio). AR grade $CaCO_3$ was obtained from Sisco Research Laboratory Pvt. Ltd. and $Al(OH)_3$ gel powder, from Loba Chemie. Based on a TG-DSC analysis of these components, the right amounts were taken so as to achieve the required mole ratio, as described in Ghoroi and Suresh.[1] The $C_{12}A_7$ powders were sieved, and the fraction passing through 45μm was collected. Similarly, in the case of $CaCO_3$, the fraction passing through a 53 μm sieve was used. These $C_{12}A_7$ and $CaCO_3$ powders were taken in appropriate amounts so as to achieve a mole ratio 1:9, and slurried in cyclohexane to achieve intimate mixing. The slurried mixture was dried in an oven maintained at 55°C. The particle-size distribution of the individual powders ($CaCO_3$ and $C_{12}A_7$), as well as the powder mixture were recorded using a GALAI CIS-1 instrument (Migdal Haemek, Israel) using methanol as a suspending medium. The dried powder mixture was then calcined at 800°C for 1h in a tube furnace. An XRD study carried out on some of the samples confirmed the complete conversion of $CaCO_3$, as well as the absence of any other reaction products. The powder mixture was then made into pellets of 12 mm dia., using an isostatically cold press at 300 MPa. All these protocols were in accordance with the conditions established in our earlier study.[1]

A programmable-temperature high-temperature chamber furnace (60 F4, Super Kanthal Okay Electric Furnace, Bysakh & Co., India), programmed for the desired temperature (in the temperature range of 1,150°C to 1,300°C) was used to carry out the reaction in the pellets in order to obtain isothermal kinetics. The furnace was heated to the desired isothermal temperature, and then the green pellets introduced. Samples were taken out after the desired time intervals, air quenched and stored in a desiccator for quantitative X-ray diffraction (QXRD) analysis.

Phase quantification was done using the Internal Standard method,[61] as described in greater detail in Ghoroi and Suresh.[1] All reacted pellets were ground using an agate mortar-and-pestle, and the sample passed through the 53 μm sieve to minimize the XRD intensity variation with particle size. A fixed amount of an internal standard (rutile, 14.65%), also sieved through the 53 μm sieve, was added to the ground and sieved sample and mixed thoroughly under cyclohexane. The mixture was then dried as before and examined by Philips X'Pert PRO diffractometer, using Cu as a target at a voltage of 40 kV, and current of 30 mA. Randomly oriented samples were prepared for X-ray diffraction by back-loading technique to avoid any preferential orientation. Scans were taken from for a 2θ range of 5–70° with a step size of 0.017°, and different phases were quantified using previously prepared calibration samples. Calibration procedures and methods of interpretation of XRD results have been detailed elsewhere.[1]

Results and Discussion

The mean size of the individual reactant particles were comparable at 2.52 μm for $CaCO_3$ (range 0.5–12.0 μm), and 1.77μm for $C_{12}A_7$ (range 0.5–8.0 μm). The reactant mixture

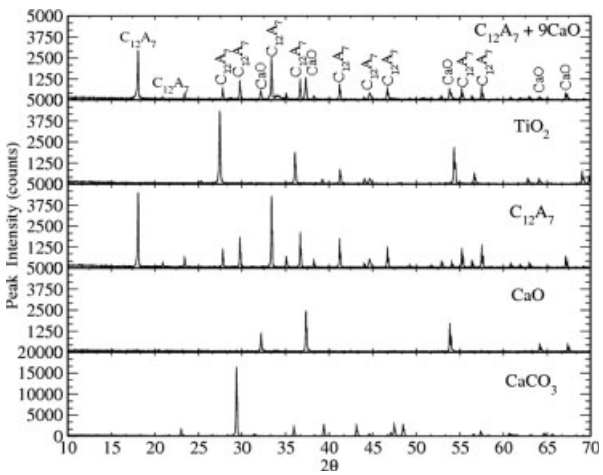

Figure 1. X-ray diffractograms of pure samples and of a mixture of $C_{12}A_7$ and $CaCO_3$ (1:9 mole ratio), calcined at 800°C for 1 h.

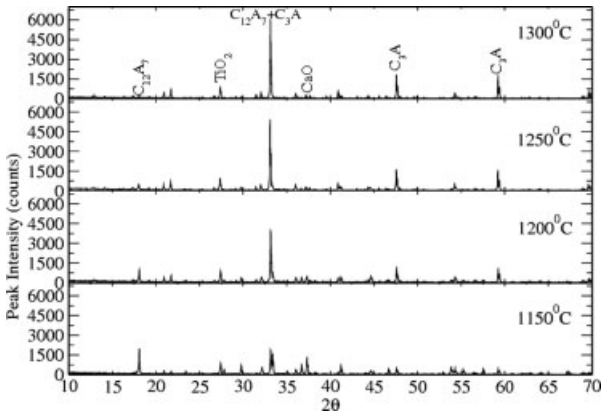

Figure 2. X-ray diffractograms of samples collected after 3 h of reaction at different temperatures.

had a mean size of 1.81 μm (range 0.5–11.0 μm). The other properties of interest are tabulated in Table 2.

The X-ray diffractograms of the different pure phases of interest, including that of the reaction mixture after calcination (showing only $C_{12}A_7$ and CaO) are shown in Figure 1. Isothermal experiments to study the kinetics of C_3A formation from $C_{12}A_7$ and CaO were performed at 1,150°C, 1,200°C, 1,250°C, and 1,300°C. A typical set of XRDs, comparing samples reacted for 3h at different temperatures, is shown in Figure 2. Mass fractions of C_3A and $C_{12}A_7$ at different times, for each of the experimental temperatures, have been calculated from such diffractograms, using the calibration curves. It proved difficult to construct reliable calibration curves for CaO because of its tendency to hydrate and form $Ca(OH)_2$. Therefore, although the signatures of CaO were distinguishable in the XRDs, its mass fractions were calculated from material balance. This procedure had been earlier tested in our experiments on the synthesis of C_3A from the oxides, against independent determinations of free CaO by titrimetric methods, and seen to give results within 2% of the latter.

Figure 3 shows the results. Some general observations are immediate. C_3A was the only new phase observed to form in every reacted sample, and no other calcium aluminate phases were observed. Figure 3 shows that the mass fraction of C_3A increases monotonically with the heating time at each temperature, levelling off at large times. Similarly, the mass fractions of $C_{12}A_7$ and CaO decrease monotonically toward zero with time. These observations indicate that the formation of C_3A from $C_{12}A_7$ and CaO can be considered to occur in a single step (Eq. 2). The increasing velocity of reaction with temperature is also obvious from the figure.

Since we are measuring the mass fractions of both $C_{12}A_7$, as well as C_3A in the reacted samples, the fraction of $C_{12}A_7$ converted can be calculated from either. We, thus, have two measures of conversion (α), one from the product (directly measured), and the other from the reactant, calculated as

$$\alpha_{C12A7} = 1 - \left(\frac{f_{C12A7,t}}{f_{C12A7,t=0}}\right) \tag{10}$$

The difference between these two calculations of conversion is taken to represent the error in the conversion measurement. Figure 4 shows the conversion-time behavior at different temperatures, with the error bars generated thus.

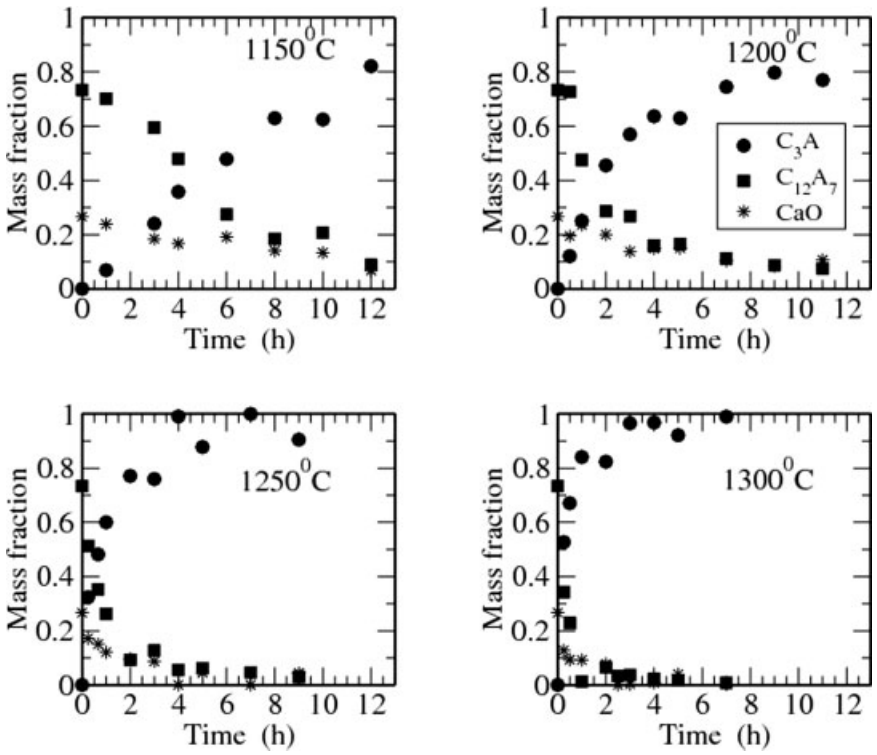

Figure 3. Variation of phase mass fractions with time at different temperatures.

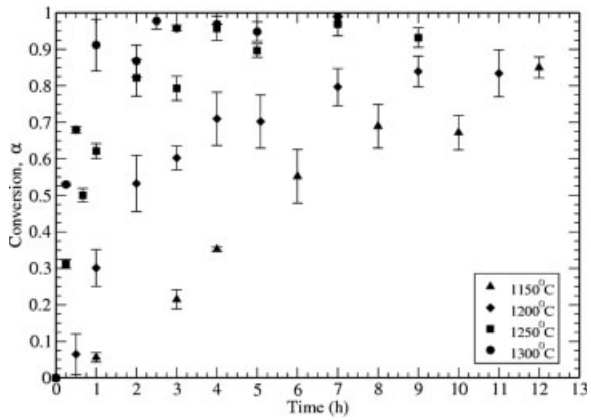

Figure 4. Average conversion with error bar vs. time plot at different temperatures.

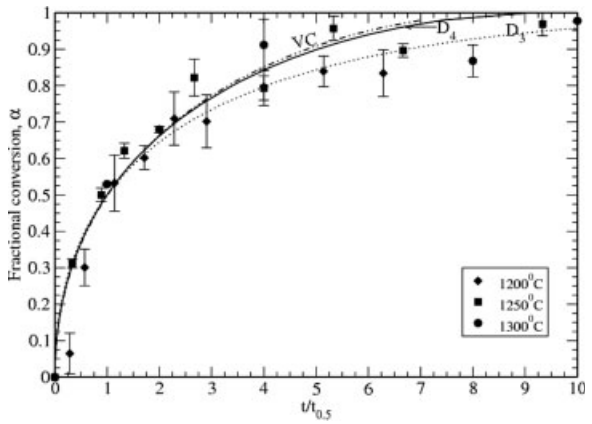

Figure 6. Reduced time plot of the conversion-time data at different temperatures, along with diffusion-controlled shrinking core models (data at 1150 C are not included).

D_3: Jander model; D_4: Ginstling-Brounshtein model; VC: Valensi-Carter model.

Kinetic parameters from the Shrinking core models

In order to examine the fit of models of the type of Eq. 1, the time for 50% conversion ($t_{0.5}$) was calculated for different temperatures from the curves of Figure 4. A reduced time plot of the experimental data is shown in Figure 5, along with several models commonly used in the literature as listed by Sharp et al.[38] From the figure, it is seen that, in general, models of the shrinking core type (R_3, D_3, D_4 and VC) fit the data better, as is to be expected from the fact that this *genre* of models is more popular than the others in fitting solid-solid reaction kinetics. The data at 1,150°C follow model R_3 (reaction control), while at higher temperatures, the data follow more closely the models assuming diffusion control (VC, D_4, D_3). For clarity, the data at these higher temperatures are replotted against the diffusion-control models in Figure 6. Considering that the Jander model treats diffusion in a slab geometry, its ability to fit high-temperature data at even high-conversions is surprising. However, since the three models differ only at high-conversions, and given the general scatter in the data, all three models may be considered to fit the data more or less equally. On mechanistic grounds, we may note that the D_4 and VC models are on better foundation than D_3, in sofar as they treat the reacting particle as spherical, which probably mimics reality better; the VC model also accounts for changes in particle size (in this case, the parameter Z works out to 1.22).

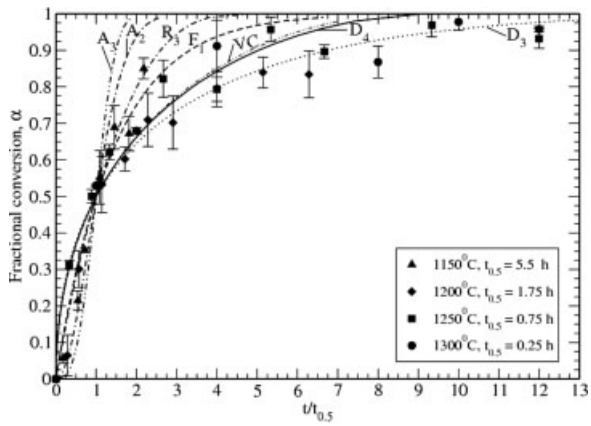

Figure 5. Reduced time plot of the conversion-time data along with some of the commonly used models listed in Sharp et al.[38]

A_3 and A_2: nucleation and growth model; R_3: reaction control model; F_1: first-order reaction model; D_3: Jander model; D_4: Ginstling-Brounshtein model; VC: Valensi-Carter model. See Sharp et al.[38] for details on models A_2, A_3, R_3 and F1.

Figure 7 shows plots of g(α) against time for the four models in contention - R_3, D_3, D_4 and VC. Note that the function plotted along the ordinate in each of these plots is different and depends on the particular model being plotted. The superior fit of R_3 for the 1,150°C data is clear. While R_3 is clearly inferior to the others at higher temperatures, it is difficult to discriminate between the other three at these temperatures. Further, the scatter of the plot at 1,300°C is such that a good fit cannot be cleanly demonstrated for any of the models.

The values of the parameter k in Eq. 1 for the different models were calculated from the slope of the best-fit lines in Figure 7 (see Table 3). These values were then used as initial guesses and refined estimates obtained by nonlinear regression on the α-t relationships, in which the function

$$\chi^2(k) = \sum_{i=1}^{N} \left[\frac{\alpha_i - \alpha(t_i; k)}{\sigma_i} \right]^2 \tag{11}$$

was minimized with respect to the parameter k. Here, α_i is the average experimental conversion at the time-point t_i, and $\alpha(t_i; k)$ is the value predicted at the same time-point by the model for the chosen value of the paramter. σ_i, the standard deviation at the i^{th} point is estimated from the two estimates of the conversion as described earlier. The predicted conversion $\alpha(t_i; k)$ was calculated by inverting the relationship in Eq. 1 (in the case of models D_4 and VC, this was done using a Newton-Raphson procedure). The subroutine MRQMIN,[64] which uses a Levenberg-Marquardt algorithm, was used to carry out the minimization. The final regressed values of k

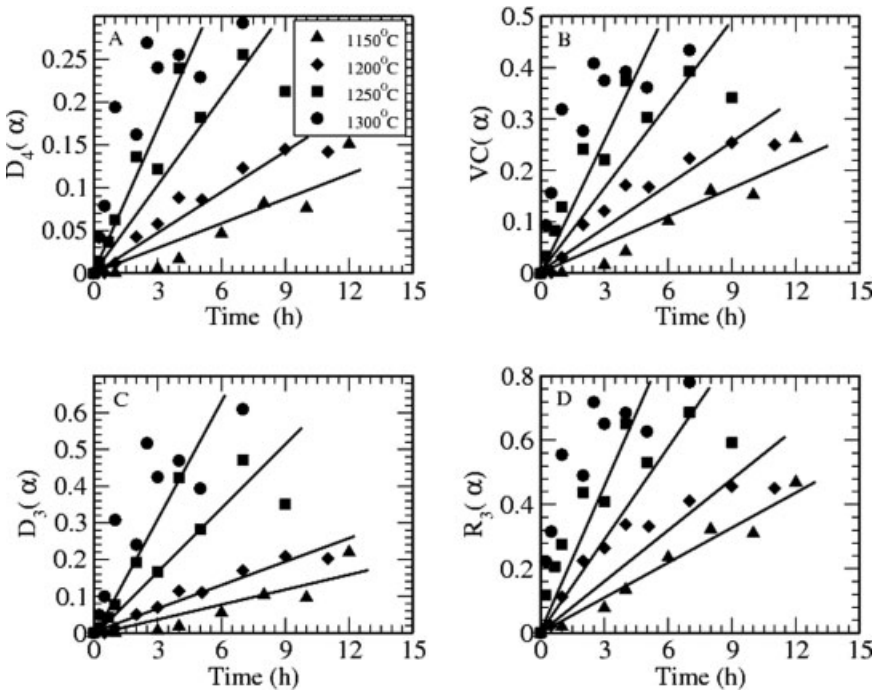

Figure 7. g(α) vs. t plot for (A) Ginstling-Brounshtein model, $D_4(\alpha)$ (B) Valensi-Carter model VC(α), (C) Jander model D_3 (α), and (D) reaction control model $R_3(\alpha)$.

are also shown in Table 3, and are in general seen to be different from the linear estimates. In cases such as the data for 1,300°C, since the data has a lot of scatter, the search space was enlarged by using additional guess values, and the minimum of all "optimized" χ^2 values was chosen.

The final regressed values of k were then used for calculating the effective diffusivity (D_e) of CaO through the product layer (reaction rate constant in the case of 1150°C data) using the physical parameters of Table 2 and the relevant expression for k (Table 1). Table 4 shows the results.

Kinetic parameters from the Ishida-Wen model

The parameters of the Ishida-Wen model may be considered to be k_P and ϕ, which between them incorporate the reaction rate constant, as well as diffusivity of B. Over the temperature range of interest, these parameters were estimated by the same "Chi-square" procedure[64] as was described in the previous section. The function to be minimized, here with respect to two parameters, was

$$\chi^2(k_P, \phi) = \sum_{i=1}^{N} \left[\frac{\alpha_i - \alpha(t_i; k_P, \phi)}{\sigma_i} \right]^2 \tag{12}$$

The subroutine MRQMIN[64] was again used to carry out the minimization. The conversion-time relationship for use in Eq.12 is given by Eq. 3 or Eq. 4 accordingly as $t < t_1$ or $t > t_1$, where t_1 itself (Eq. 6) is determined by one of the (unknown) parameters. This created some problems for the routine when a two parameter estimation was attempted, and the following procedure was adopted. One of the parameters (parameter 1, usually D_e) was fixed (at about the value estimated for the earlier models), and the other parameter (parameter 2, usually ϕ) was estimated using MRQMIN. The value of χ^2 at the minimum was noted. The procedure was repeated for several assumed values of parameter 1, and a plot of the "minimum" χ^2 vs. parameter 1 was made to locate the "global" minimum. The corresponding values of parameter 1 and parameter 2 were picked up as the estimates

Table 3. Rate Parameters ($k \times 10^5$ s^{-1}) Regressed from the Shrinking Core Models at Different Temperatures (L: Linear Estimate and NL: Nonlinear Estimate)

	Models							
	D_3		D_4		VC		R_3	
Temperature	L	NL	L	NL	L	NL	L	NL
1150°C	—	—	—	—	—	—	1.01	0.93
1200°C	0.60	0.58	0.43	0.46	0.48	0.52	—	—
1250°C	1.58	1.77	0.94	1.40	1.01	1.62	—	—
1300°C	3.90	3.42	1.55	4.63	1.67	5.34	—	—

Table 4. Diffusivity ($D_e \times 10^{18}$ m^2 s^{-1}) or Reaction Rate Constant ($k_s \times 10^{12}$ m s^{-1}) Estimated from the Regressed Values of k in Table 3

	Models			
	D_e			k_s
Temperature	D_3	D_4	VC	R_3
1150°C	—	—	—	1.21
1200°C	0.67	0.53	0.55	—
1250°C	2.04	1.61	1.86	—
1300°C	3.94	5.34	6.15	—

Only nonlinear estimates have been used.

Table 5. Fitted Parameters using Ishida-Wen Model

Temperature	φ	k_P (m^3 $kmol^{-1}$ s^{-1})	D_e (m^2 s^{-1})
1150°C	4.4	7.8×10^{-7}	5.40×10^{-19}
1200°C	11.0	5.45×10^{-6}	6.16×10^{-19}
1250°C	34.24	1.41×10^{-4}	1.65×10^{-18}
1300°C	35.24	4.82×10^{-4}	5.48×10^{-18}

for that set of data. For the data at 1,150°C, since the earlier estimation procedures have indicated reaction rather than diffusion control, k_P was kept fixed as parameter 1 in the initial tracking of local minima, and estimated later through the plot of these local minima as a function of the assumed k_P. As in the earlier case, the parameter values at 1,300°C should be regarded as more approximate than at the lower temperatures because of the scatter in the data; the problem manifested itself as a broad minimum in the second part of the parameter estimation exercise described before. The parameter values (ϕ, k_P and D_e) at the different temperatures are summarized in Table 5. The higher the temperature, the higher the value of ϕ, indicating the increasing severity of diffusion limitation (and, hence, an increasing tendency for the reaction to become confined to a front) as temperature increases. This is also clear from the rather similar values of diffusivity as estimated from the front-reaction models and the Ishida-Wen model at the higher temperatures.

The success of the front-reaction (shrinking-core) models can now be explained, at least in some cases, in the light of the more general Ishida-Wen model. For this purpose, a (dimensionless) reaction zone "thickness" has been estimated from the Ishida-Wen model as the difference between ξ_m, and the value of the dimensionless radius at which the concentration of B drops to 1% of its maximum (surface) value. Figure 8 shows this thickness ($\xi_m - \xi_{0.01CB0}$) as a function of time. Clearly, little error results if the reaction at 1,250°C and above is considered to take place at a "front", since at these temperatures, very soon the reaction zone becomes thin enough as to be indistinguishable from a surface. Thus, models such as D_4 and VC would be quite accurate under these circumstances. At the lower temperatures, however, the fit of the models should be regarded as more of a coincidence as Figure 8 demonstrates.

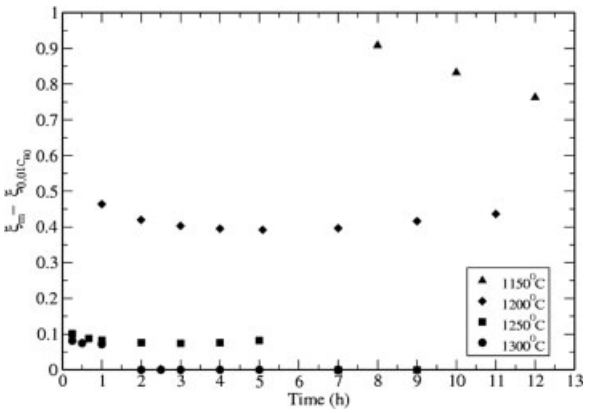

Figure 8. Reaction layer thickness vs. time as calculated from the Ishida-Wen model.

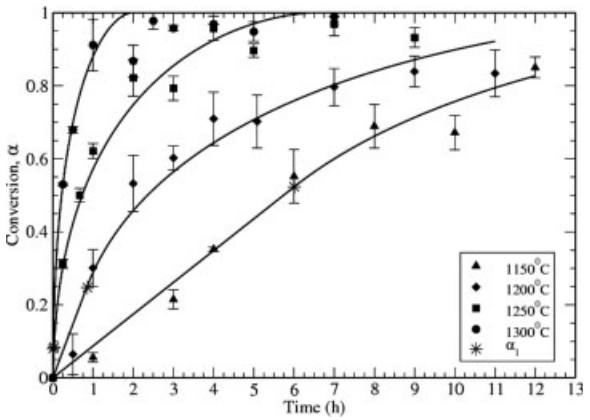

Figure 9. Fitted conversion vs. time plot as calculated from Ishida-Wen model.

The conversion vs. time behavior as predicted by the Ishida-Wen model with the fitted parameters is shown compared with the data in Figure 9. The end of the first stage (α_1 and t_1) is also marked in the figure. The values of χ^2 for the regressed parameter set, were substantially lower than for the shrinking core models at 1,150° and 1,200°C, while being comparable at the two higher temperatures.

Kinetic parameters from the contact-point model

The contact point model has the diffusivity of B as the parameter to be estimated, and this is hidden in the constant K used in the definition of dimensionless time (Eq. 8). The following procedure was followed to estimate K. From the initial volume fraction of the immobile reactant X_{VI} in the reaction mixture and the ratio of initial particle radii, the number of contact points N_{cp} was calculated using the expression given by Hao and Tanaka.[49] This gave a value of 2.3. Since N_{cp} has to be an integer, calculations were performed for both $N_{cp} = 2$, and $N_{cp} = 3$. The values of the parameters κ and n in Eq. 9 for the chosen N_{cp} were found from Hao and Tanaka,[49] and the dimensionless time τ_1, at which the transition period ends was calculated[49] from $(\tau_1)^{\frac{1}{3}} = \frac{2}{N_{cp}}\sqrt{N_{cp}-1}$. These values, constant for all our experiments and independent of temperature, are shown in Table 6. The α-τ curve, valid for all temperatures, could now be drawn from Eqs. 7 and 9. A value of K was now estimated for each temperature from the x-shift required to match this curve with the experimental data for the temperature. Using this as the initial guess, a refined value of K was regressed once again using the routine MRQMIN, as described above. Figure 10 shows the fit of the data with the regressed values of K. From the value of K, the value of D_e was calculated using the property values listed in Table 2. These values are shown in Table 7.

Table 6. Parameters for the Contact Point Model. $N_{cp} = 2$ and 3

N_{cp}	τ_1	α_1	κ	n
$N_{cp} = 2$	1.0	0.62	0.98	1.5
$N_{cp} = 3$	0.83	0.81	2.3	1.8

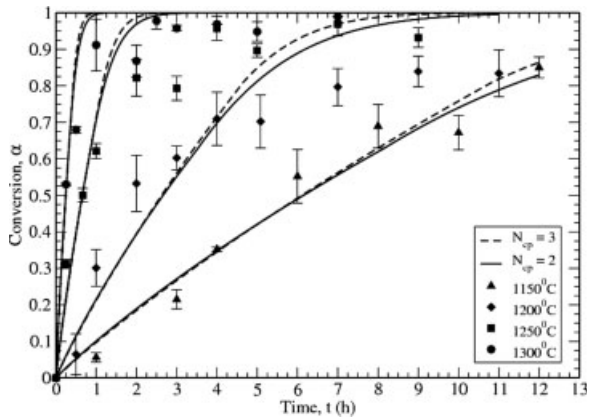

Figure 10. Fitted conversion vs. time plot as calculated from contact point model.

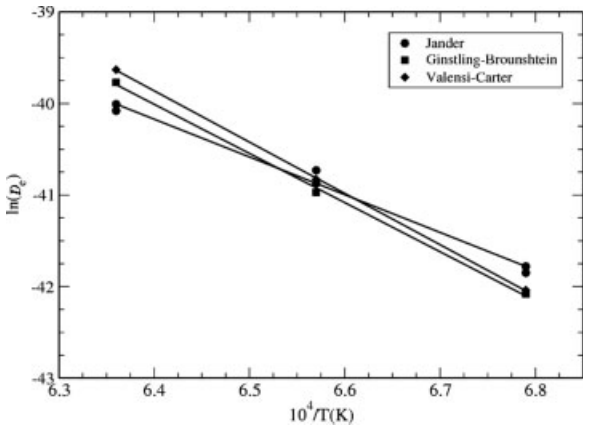

Figure 11. ln(D_e) vs. 10^4/T plot for diffusion control models — Ginstling-Brounshtein model (D_4), Valensi-Carter model (VC), and Jander model (D_3) in the temperature range of 1,200–1,300°C.

Activation energies according of different models

Activation energies for the relevant kinetic parameter (diffusivity or rate constant) can be determined in the conventional manner, through the appropriate Arrhenius plots. For the shrinking core models, such plots are shown in Figure 11 for D_e (since this is the only parameter available over a temperature range, values being available for three temperatures). The Ishida-Wen model gives a value for each of diffusivity and (homogeneous) rate constant, and activation energy plots for both of these are shown in Figure 12. The contact point model does not permit anything but diffusion control, and the estimated diffusivity values at the four temperatures have been used in Figure 13 to calculate activation energy. Both 2 and 3 contact point cases are shown. The activation energy (and pre-exponential factor) values for the different models and parameters are compared in Table 8.

Ghoroi and Suresh[1] in their work on calcia-alumina reactions leading to C_3A, compared the values of activation energies reported by different authors for diffusivities in the calcia-alumina couple. A look at their comparison shows that values of activation energies are usually around 200 kJ mol^{-1}. It is only the Ishida-Wen model which predicts an activation energy for diffusivity that is close to this figure. Further in this model, the activation energy for the rate constant is much higher than that for diffusivity, as is to be expected.

Conclusions

The reaction between $C_{12}A_7$ and CaO, one of the reactions in the formation of C_3A from the oxides of calcium and aluminum, has been studied in this work, over a temperature range of 1,150–1,300°C. These results, taken together with the results reported in our earlier work[1] would help interpret the complete kinetics of conversion of alumina and calcia to C_3A. Our results show that the conversion of $C_{12}A_7$ to C_3A occurs in a single step, with no intermediates being detected.

In addition to obtaining the kinetics of the reaction of interest, the latter has been used as a case study to address some general issues in the modeling of solid-solid reactions. To this end, the experimental results have been interpreted in terms of the traditionally used front-reaction models, such as those due to Jander, Ginstling-Brounshtein and Valensi-Carter, and also with some rarely used models, such as the Ishida-Wen model and the contact-point model. The front-reaction models have been inspired by the fluid-solid literature, and considering the differences between those systems and solid-solid systems, their extensive use in the latter over several decades is rather surprising. The question that bothers

Table 7. Diffusivity Values Calculated from Contact Point Model

	D_e (m^2 s^{-1})	
Temperature	$N_{cp} = 2$	$N_{cp} = 3$
1150°C	1.11×10^{-16}	6.95×10^{-17}
1200°C	2.57×10^{-16}	1.61×10^{-16}
1250°C	1.05×10^{-15}	6.44×10^{-16}
1300°C	2.82×10^{-15}	1.73×10^{-15}

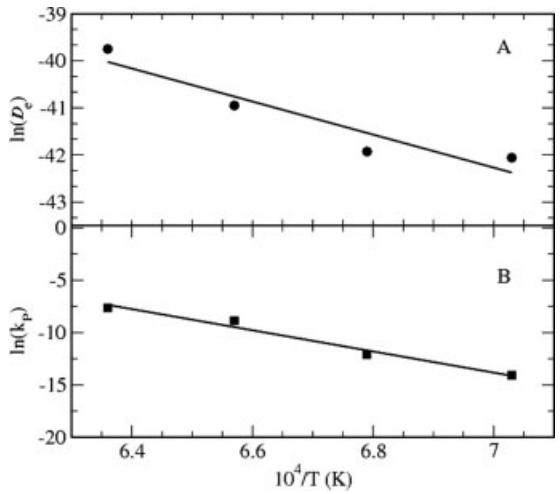

Figure 12. (A): ln(D_e) vs (10^4/T) plot and (B): ln(k_P) vs. (10^4/T) plot for the Ishida-Wen model.

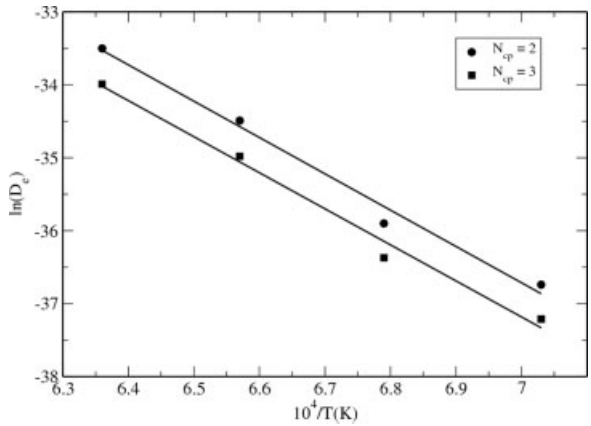

Figure 13. ln(D_e) vs. (10^4/T) plot for the contact point model for 1150^0–1300°C.

one is, therefore, whether these models just happen to provide fitting equations which mimic the conversion-time behavior in solid systems. Indeed, this work shows that it is possible to fit the data (albeit with varying degrees of goodness) with *any* of the models used. Of the models that treat the diffusing phase as a continuum, the Ishida-Wen model may be considered more general than the others, in that it incorporates the Ginstling-Brounshtein model as a special case. The interpretation of our data using this model explains in some measure the success of the front models, since the reaction zone under some circumstances could be thin enough that the assumption of a reaction front is a good one. However, there could be circumstances in solid-solid reactions in which the volume reaction would have an important role to play. Our results clearly show a transition from one to the other as the temperature is varied. A strong case is, thus, made for considering volume reaction models in the solid-solid context. So far as the system in question is concerned, these results qualitatively explain the experimentally observed accumulation of the intermediate in our earlier work.[1]

The contact point model provides an alternative viewpoint to model reactions in particulate systems, that is more attractive than the continuum models as a modeling philosophy. However, in the current state of its development, it suffers from disadvantages that, in our opinion, are a result of the assumptions made to keep the geometrical details tractable. These disadvantages show up particularly in cases where the estimated number of contact points is small, such as this case, as shown by the considerably poorer performance of the model in comparison with the others. It would be interesting to develop models within this framework that allow for volume reaction, and work is in progress in that direction.

Table 8. Activation Energy (E) and Pre-exponential Factor (A) for the Kinetic Parameters Estimated for the Different Models

Model	A	E (kJ mol^{-1})
Ishida-Wen model, D_e	2.16×10^{-8}	293
Ishida-Wen model, k_P	4.90×10^{24}	840
Ginstling-Brounshtein model, D_e	3.03×10^{-3}	445
Valensi-Carter model, D_e	1.67×10^{-2}	465
Jander model, D_e	9.70×10^{-7}	342
Contact point model, $N_{cp} = 2$, D_e	1.41×10^{-1}	413
Contact point model, $N_{cp} = 3$, D_e	6.80×10^{-2}	410

The units of A are m^2 s^{-1} for diffusivities and m^3 kmol^{-1}s^{-1} for k_P.

Acknowledgments

One of the authors (CG) was supported for a large part of this work through a project funded by the Council of Scientific and Industrial Research (CSIR), Goverment of India.

Notation

A = pre-exponential factor, pre-exponential factor, m^{2}s^{-1} or m^3 kmol^{-1}s^{-1}
C = concentration, kmol.m^{-3}
D_e = effective diffusivity of B through composite product layer, m^2 s^{-1}
E = activation energy, kJ mol^{-1}
f = fraction
k_P = reaction rate constant of product P formation by volume reaction, m^{3}kmol^{-1}s^{-1}
k_s = reaction rate constant for surface reaction, m.s^{-1}
k = reaction rate parameter, s^{-1}
N = number of experimental data points
N_{cp} = number of contact points
R_{I0} = initial radius of particle I, m
t = time, s
$t_{0.5}$ = time in at which conversion is 50%, s
T = temperature, in K
Z = volume of product formed from unit volume of reactant

Greek letters

α = fractional conversion
θ = angle in degree
χ^2 = merit function in Levenberg-Marquardt method
ν = stoichiometric coefficients
ϕ = thiele modulus
σ_i = standard deviation in conversion of ith data point
τ = dimensionless time in contact point model
ξ = radius ratio at any time, t within the particle I, $(= \frac{r}{R_{I0}})$
ξ_m = radius ratio at the end of the first stage in Ishida-Wen model
$\xi_{0.01CB0}$ = radius ratio where C_B = 1.0% of C_{B0}

Subscripts

1 = end of first stage
B = reactant B
$B0$ = B at outer surface of I
cp = contact point
$I0$ = I at initial period

Literature Cited

1. Ghoroi C, Suresh AK. Solid-solid reaction kinetics - Formation of tricalcium aluminate. *AIChE J*. 2007;53:502–513.
2. Taylor HFW. Cement Chemistry. London: Academic Press; 1964.
3. Yang S, Kondo JN, Hayashi K, Hirano M, Domen K, Hosono H. Partial oxidation of methane to syngas over promoted $C_{12}A_7$. *Appl Catal A: General*. 2004;277:239–246.
4. Oh SH, Finones R, Choi SY, Kim KN. Influence of tricalcium aluminate phase on *in vitro* biocompatibility of calcium aluminate bone cement. *J Mat Res*. 2004;19:1062–1067.
5. Suresh. AK. Thermal Analysis in the investigation of multi-step reactive process - Applications and some issues. In: Rama Rao GA, Parida SC, Ravindran PV, Bharadwaj SR, Venugopal V. *Proceedings of the Fifteenth National Symposium on Thermal Analysis*. Jaipur: Bhabha Atomic Research Center; 2006:40–46.

6. Mohamed BM, Sharp JH. Kinetics and mechanism of formation of tricalcium aluminate, $Ca_3Al_2O_6$. *Thermochimica Acta*. 2002;338: 105–114.
7. Marinichev VS, Rumyantsev PF. The kinetics of formation of calcium aluminate ($12CaO.7Al_2O_3$). *Neorganicheskie Materialy*. 1988; 24:810–813.
8. Mohamed BM, Sharp JH. Kinetics of formation of $Ca_{12}Al_{14}O_{33}$ (dodecacalcium heptaaluminate). In: Mangabhai RJ, Glasser, FP. *Proceedings of the International Conference on Calcium Aluminate Cements*. Edinburgh, Scotland, UK; 2001:65–76.
9. Hao YJ, Tanaka T. Prediction of the diffusing component(s) in a solid-solid reaction system. *Solid State Ionics*. 1990;38:213–216.
10. Hao YJ, Tanaka T. A new experimental method to specify the diffusing component in reacting particulate packing. *Canadian J of Chem Eng*. 1990;68:81–88.
11. Tagai H, Iseki T, Saeki T, Kounosu, T. Solid state reaction between calcium oxide and aluminium oxide single crystal. *Yogyo Kyokaishi*. 1969;77:341–347.
12. Tamhankar SS, Doraiswamy LK. Analysis of solid-solid reactions: A review. *AIChE J*. 1979;25:561–582.
13. Sasaki H. Introduction to particle size distribution into kinetics of solid-state reaction. *J Am Cerm Soc*. 1964;47:512–517.
14. Komatso W. Kinetic equation of the solid state reaction: The effect of particle size and mixing ratio on the reaction rate in a mixed powder system. In: Schwab GM. *Reactivity of solids*. Munich: Elsevier Publishing Company; 1964:183–191.
15. Gallagher KJ. The Effect of particle size distribution on the kinetics of diffusion reactions in powders. In: Schwab GM. *Reactivity of solids*. Munich: Elsevier Publishing Company; 1964:192–203.
16. Kapur PC. Kinetics of solid state reactions of particulate ensembles with size distributions. *J Am Cerm Soc*. 1973;56:79–81.
17. Beretka J, Brown T. Effect of particle size on the kinetics of the reaction between magnesium and aluminium oxide. *J Am Cerm Soc*. 1983;66:383–388.
18. Urrutia GA, Miguel AB. The influence of particle size distribution on the conversion/time profiles under contracting-geometry kinetic regimes. *Reactivity of Solids*. 1988;6:281–284.
19. Koga N, Criado JM. Kinetic analysis of solid-state reactions with a particle-size distribution. *J Am Cerm Soc*. 1998;81:2901–2909.
20. Valensi G. Kinetics of the oxidation of metallic wires. *Compt Rend Acad Sci*. 1935;201:602–604.
21. Valensi G. Kinetics of oxidation of metallic spherules and powders. *Compt Rend Acad Sci*. 1936;202:309–312.
22. Valensi G. Analysis of the methods of interpreting reactions of a gas with a solid to form another solid. *J Chim Phys-Chim Bio*. 1950; 47:489–505.
23. Carter RE. Kinetic model for solid state reaction. *J Chem Phys*. 1961;34:2010–2015.
24. Carter RE. Addendum: Kinetic model for solid state reaction. *J Chem Phys*. 1961;35:1137–1138.
25. Jander W, Hoffman E. Reaction in solid state at higher temperature: XI. The reaction between calcium oxide and silicon oxide. *Z Anorg Allgen Chem*. 1934;218:211–223.
26. Arrowsmith RJ, Smith JM. Diffusion and reaction in solids. *Ind Eng Chem. Fundamentals*. 1966;5:327–335.
27. Kohatsu I, Brindley GW. Solid state reactions between calcium oxide and α-aluminium oxide. *Zeitschrift fuer Physikalische Chemie*. 1968;60:79–89.
28. Shatynski SR, Hirth JP, Rapp RA. A theory of multiphase binary diffusion. *Acta Metallurgica*. 1976;24:1071–1078.
29. Tamhankar SS, Doraiswamy LK. Solid-solid reactions: Diffusion and reaction in pellet-pellet system. *Ind Eng Chem Fundamentals*. 1978;17:84–89.
30. Kostogorova J, Viljoen HJ, Shteinberg A. Role of particle geometry and surface contacts in solid-phase reactions. *AIChE J*. 2002;48: 1794–1803.
31. Fatu D. Factors on which the rate of solid-solid reactions depends. *Thermochimica Acta*. 1991;177:15–21.
32. Jander W. Reaction in the solid state at high temperatures. I. Rate of reaction for an endothermic change. *Z Anorg Allgen Chem*. 1927; 163:1–30.
33. Ginstling AM, Brounshtein BL. Concerning the diffusion kinetics of reactions in spherical particles. *J Appl Chem of U.S.S.R*. 1950;23: 1327–1338.
34. Doraiswami LK, Sharma MM. *Gas-solid non catalytic reactions: Analysis and modeling in Heterogeneous reactions; I*: Wiley-Interscience Publication; 1984.
35. Beretka J. Kinetic analysis of solid-state reactions between powdered reactants. *J Am Cerm Soc*. 1984;67:615–620.
36. Mukherjee JL, Wang FFY. Kinetics of solid state reaction of Bi_2O_3 and Fe_2O_3. *J Am Cerm Soc*. 1971;54:31–34.
37. Watanabe, K., "Kinetics of solid-state reaction of BaO_2 and α - Fe_2O_3. *J Am Cerm Soc*. 1981;81:733–737.
38. Sharp JH, Brindley GW, Achar BNN. Numerical data for some commonly used solid state reaction equations. *J. Amer. Cerm. Soc*. 1966; 49:379–382.
39. Ishida M, Yoshino K, Shirai T. The applicability of the pesudo-steady state approximation to moving boundary problems for spheres. *J Chem Eng of Japan*. 1970;3:47–54.
40. Lindman N, Simonsson D. On the application of the shrinking core model to liquid - solid reactions. *Chem Eng Sci*. 1979;34:31–35.
41. Huang PGY, Lu CH, Sheu TWH. Numerical simulation of diffusion-controlled solid-state reactions in spherical particles. *Materials Sci & Eng B: Solid-State Materials for Adv Technol*. 2004;B107:39–45.
42. Frade JR, Cable M. Reexamination of basic theoretical model for the kinetics of solid-state reactions. *J Am Cerm Soc*. 1992;75:1949–1957.
43. Frade JR, Cable M. Numerical solutions for mixed control of powder reactions for spherical, cylindrical, or planer particle. *J Am Cerm Soc*. 1995;78:90–96.
44. Frade JR, Cable M. Theoretical solutions for mixed control of solid state reactions. *J Materials Sci*. 1997;32:2727–2733.
45. Ishida M, Wen CY. Comparison of kinetic and diffusional models for solid-gas reactions. *AIChE J*. 1968;14:311–317.
46. Ishida M, Wen CY. Comparison of zone-reaction-model and unreacted-core shrinking model in gas solid reactions-I: Isothermal analysis. *Chem Eng Sci*. 1971;26:1031–1041.
47. Ouchiyama N, Tanaka T. Estimaiton of the average number of contacts between randomly mixed solid particles. *Ind Eng Chem Fundam*. 1980;19:338–340.
48. Hao YJ, Tanaka T. Role of contact points between particles on the reactivity of solids. *Canadian J of Chem Eng*. 1988;66:761–766.
49. Hao YJ, Tanaka T. Analysis of a solid-solid reaction controlled by unidirectional diffusion. *Int Chem Eng. (English Trans.)*. 1990; 30: 224–253.
50. Shimizu A, Hao YJ. Influence of particle contact on the estimation of powder reaction kinetics of binary mixtures. *J Am Cerm Soc*. 1997;80:557–568.
51. Shimizu A, Saitou J, Hao YJ. Effect of contact points between particles on the reaction rate in the Fe_2O_3 - V_2O_5 system. *Solid State Ionics*. 1990;38:261–269.
52. Shimizu A, Hao YJ, Tanaka T. Representation of concentric spherical powder reaction model in the form of linear regration analysis. *Canadian J of Chem Eng*. 1998;76:69–75.
53. Nurse RW, Welch JH, Majumdar AJ. The $12CaO.7Al_2O_3$ phase in the CaO -Al_2O_3 syatem. *Trans of British Ceramic Soc*. 1965;64: 323–332.
54. Bartl H, Scheller T. Structure of 12CaO7Al2O3. *Neues Jahrbuch fuer Mineralolie, Monatshefte*. 1970;12:547–552. (As quoted in AMCSD, http://rruff.geo.arizona.edu/AMS/amcsd.php).
55. Trofymluk O, Toda Y, Hosono H, Navrotsky A. Energetics of formation and oxidation of microporous calcium aluminates: A new class of electrides and ionic conductors. *Chem Mater*. 2005;17: 5574–5579.
56. Sushko PV, Shluger AL, Hayashi K, Hirano M, Hosono H. Mechanisms of oxygen ion diffusion in a nanoporous complex oxide $12CaO.7Al_2O_3$. *Physical Rev B: Condensed Matter and Mater Phys*. 2006;73:1–10.
57. Imlach JA, Glasser LSD, Glasser FP. Excess oxygen and the stability of 12CaO.7Al2O3. *Cement and Concrete Res*. 1971;1:57–61.
58. Hallstedt B. Assessment of the CaO - Al_2O_3 system. *J Am Cerm Soc*. 1990;73:15–23.

59. Hayashi K, Hirano M, Hosono H. Thermodynamics and kinetics of hydroxide ion formation in $12CaO.7A_{l2}O_3$. *J Phys Chem B*. 2005;109:11900–11906.
60. Singh VP, Glasser FP. High-temperature reversible moisture uptake in calcium aluminate, $Ca_{12}Al_{14}O_{33-x}(OH)_{2x}$. *Ceramics Intl*. 1988;14:59–62.
61. Chung HF, Smith DK. *Industrial applications of X-ray diffraction*. New York: Marcel Dekker; 2000.
62. Lea FM. *The Chemistry of Cement and Concrete*. Glasgow: Edward Arnold, Ltd.; 1970.
63. Chou KS, Burnet G. Formation of calcium aluminates in the lime-sinter process, Part-II: Kinetic study. *Cement and Concrete Res*. 1981;11:167–174.
64. Press WH, Teukolsky SA, Vetterling WT, Flannery BP. *Numerical recipes in FORTRAN: The art of scientific computing*. Cambridge: Cambridge University Press; 1992.

Manuscript received Mar. 6, 2007, and revision received Apr. 29, 2007.